

Topotactic desolvation and condensation reactions of 3D $\text{Zn}_3\text{TiF}_7(\text{H}_2\text{O})_2(\text{taz})_3\cdot\text{S}$ ($\text{S} = 3\text{H}_2\text{O}$ or $\text{C}_2\text{H}_5\text{OH}$)

M. Albino, J. Lhoste,* M. Body, C. Legein, A. Hémon-Ribaud, V. Maisonneuve and M. Leblanc

Electronic Supplementary Information

Table of contents

Fig. S1. 2D representation of (a) <i>trans</i> - $\text{Zn}_3\text{TiF}_7(\text{H}_2\text{O})_2(\text{taz})_3\cdot 3\text{H}_2\text{O}$ (1) and (b) <i>cis</i> - $\text{Zn}_3\text{TiF}_7(\text{H}_2\text{O})_2(\text{taz})_3\cdot \text{C}_2\text{H}_5\text{OH}$	3
Fig. S2. ORTEP representation of the asymmetric unit of (a) <i>trans</i> - $\text{Zn}_3\text{TiF}_7(\text{H}_2\text{O})_2(\text{taz})_3\cdot 3\text{H}_2\text{O}$ (1) and (b) <i>cis</i> - $\text{Zn}_3\text{TiF}_7(\text{H}_2\text{O})_2(\text{taz})_3\cdot \text{C}_2\text{H}_5\text{OH}$ (4)	3
Fig. S3. (a) TGA under humid air atmosphere, (b) thermal evolution of IR spectra and (c) thermal evolution of the powder X-Ray diffractograms of 5	4
Table S1. Experimental and PBE-DFT geometry-optimized fractional atomic coordinates and corresponding atomic displacements for phase 1 .	5
Table S2. Experimental and PBE-DFT geometry-optimized fractional atomic coordinates and corresponding atomic displacements for phase 3 .	6
Table S3. Experimental and PBE-DFT geometry-optimized fractional atomic coordinates and corresponding atomic displacements for phase 4o .	7
Table S4. Experimental and PBE-DFT geometry-optimized fractional atomic coordinates and corresponding atomic displacements for phase 7 .	8
Table S5. Experimental and PBE-DFT geometry-optimized fractional atomic coordinates and corresponding atomic displacements for phase 5p .	8
Table S6. Selected interatomic distances from ES and APO structures of phase 1 .	9
Table S7. Selected interatomic distances from ES and APO structures of phase 3 .	9
Table S8. Selected interatomic distances from ES and APO structures of phase 4o .	10
Table S9. Selected interatomic distances from ES and APO structures of phase 7 .	10
Table S10. Selected interatomic distances from ES and APO structures of phase 5p .	11
Table S11. Phase, H site and multiplicity, ^1H σ_{iso} issued from DFT-GIPAW calculations, H environment, weighted average ^{19}F σ_{iso} and corresponding relative intensity for APO structures.	12
Table S12. Phase, F site and multiplicity, ^{19}F σ_{iso} and σ_{csa} issued from DFT-GIPAW calculations, F environment, weighted average ^{19}F σ_{iso} and corresponding relative intensity for APO structures.	13
Fig. S4. Experimental ^1H MAS NMR (7 T) spectra of phases 1 , 3 , 4 and 7 recorded at 64 kHz and 44 kHz spinning frequencies.	14
Fig. S5. Experimental and fitted ^1H MAS NMR spectra of phase 1 .	15
Table S13. ^1H isotropic chemical shift, line width, relative intensity, weighted average ^1H isotropic chemical shift and corresponding relative intensity determined from reconstruction of the ^1H NMR spectrum of phase 1 .	15
Fig. S6. Experimental and fitted ^1H MAS NMR spectra of phase 3 .	16
Table S14. ^1H isotropic chemical shift, line width, relative intensity, weighted average ^1H isotropic chemical	16

shift and corresponding relative intensity determined from reconstruction of the ^1H NMR spectrum of phase **3**.

Fig. S7. Experimental and fitted ^1H MAS NMR spectra of phase **4**.

17

Table S15. ^1H isotropic chemical shift, line width, relative intensity, weighted average ^1H isotropic chemical shift and corresponding relative intensity determined from reconstruction of the ^1H NMR spectrum of phase **4**.

17

Fig. S8. Experimental and fitted ^1H MAS NMR spectra of phase **7**.

18

Table S16. ^1H isotropic chemical shift, line width, relative intensity, weighted average ^1H isotropic chemical shift and corresponding relative intensity determined from reconstruction of the ^1H NMR spectrum of phase **7**.

18

Fig. S9. $^1\text{H} \sigma_{\text{iso},\text{cal}}$ weighted average versus $^1\text{H} \delta_{\text{iso},\text{exp}}$ weighted average values.

19

Fig. S10. Experimental ^{19}F MAS NMR (7 T) spectra of phases **1**, **3**, **4** and **7** recorded at 64 kHz and 44 kHz spinning frequencies.

20

Fig. S11. Experimental and fitted ^{19}F MAS NMR spectra of phase **1**.

21

Table S17. ^{19}F isotropic chemical shift, chemical shift anisotropy, asymmetry parameter, line width, relative intensity, weighted average ^{19}F isotropic chemical shift and its corresponding relative intensity determined from reconstruction of the ^{19}F NMR spectrum of phase **1**.

21

Fig. S12. Experimental and fitted ^{19}F MAS NMR spectra of phase **3**.

22

Table S18. ^{19}F isotropic chemical shift, chemical shift anisotropy, asymmetry parameter, line width, relative intensity, weighted average ^{19}F isotropic chemical shift and its corresponding relative intensity determined from reconstruction of the ^{19}F NMR spectrum of phase **3**.

22

Fig. S13. Experimental and fitted ^{19}F MAS NMR spectra of phase **4**.

23

Table S19. ^{19}F isotropic chemical shift, chemical shift anisotropy, asymmetry parameter, line width, relative intensity, weighted average ^{19}F isotropic chemical shift and its corresponding relative intensity determined from reconstruction of the ^{19}F NMR spectrum of phase **4**.

23

Fig. S14. Experimental and fitted ^{19}F MAS NMR spectra of phase **7**.

24

Table S20. ^{19}F isotropic chemical shift, chemical shift anisotropy, asymmetry parameter, line width, relative intensity, weighted average ^{19}F isotropic chemical shift and its corresponding relative intensity determined from reconstruction of the ^{19}F NMR spectrum of phase **7**.

24

Fig. S15. $^{19}\text{F} \sigma_{\text{iso},\text{cal}}$ weighted average values versus $^{19}\text{F} \delta_{\text{iso},\text{exp}}$ weighted average values.

25

Table S21. Experimental (x, y, z) fractional atomic coordinates for phase **2**.

26

Table S22. Experimental (x, y, z) fractional atomic coordinates for phase **6**.

27

1. Representation of *trans*- and *cis*-Zn₃TiF₇(H₂O)₂(taz)₃·H₂O (5)

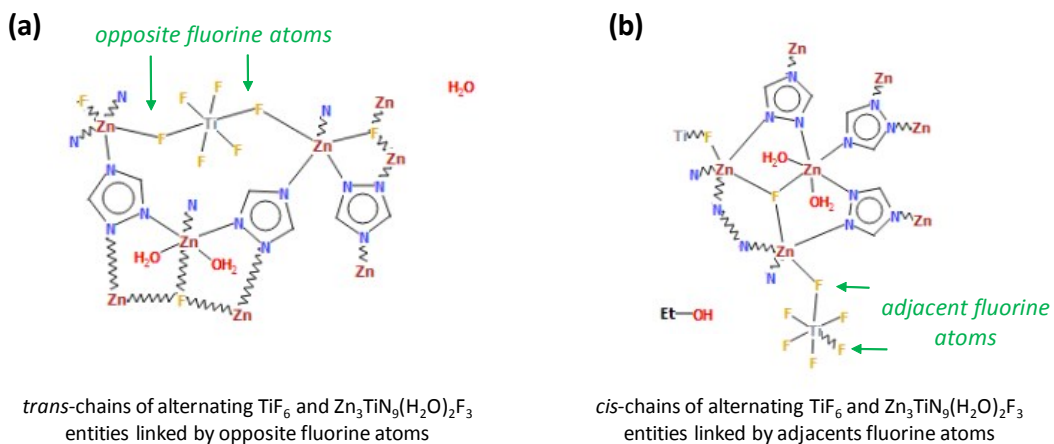


Fig. S1. 2D representation of (a) *trans*-Zn₃TiF₇(H₂O)₂(taz)₃·3H₂O (**1**) and (b) *cis*-Zn₃TiF₇(H₂O)₂(taz)₃·C₂H₅OH (**4**)

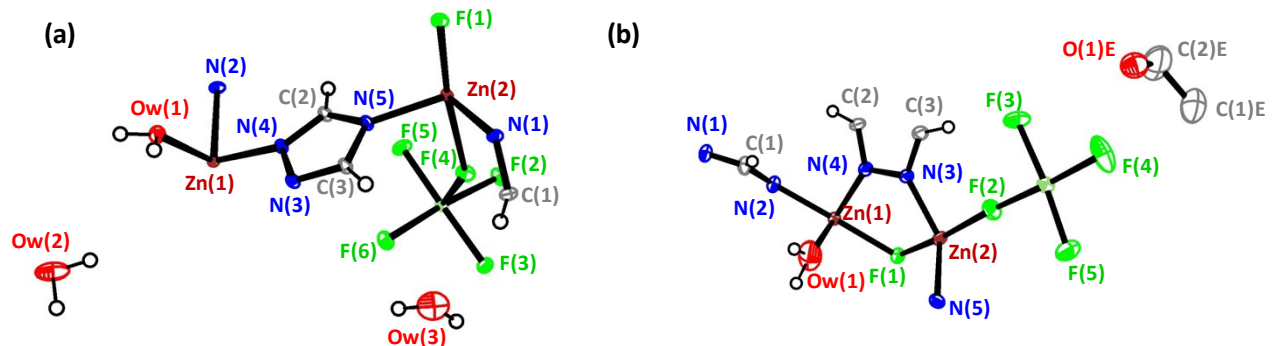


Fig. S2. ORTEP representation of the asymmetric unit of (a) *trans*-Zn₃TiF₇(H₂O)₂(taz)₃·3H₂O (**1**) and (b) *cis*-Zn₃TiF₇(H₂O)₂(taz)₃·C₂H₅OH (**4**)

2. Characterization of $cis\text{-Zn}_3\text{TiF}_7(\text{H}_2\text{O})_2(\text{taz})_3\cdot\text{H}_2\text{O}$ (5)

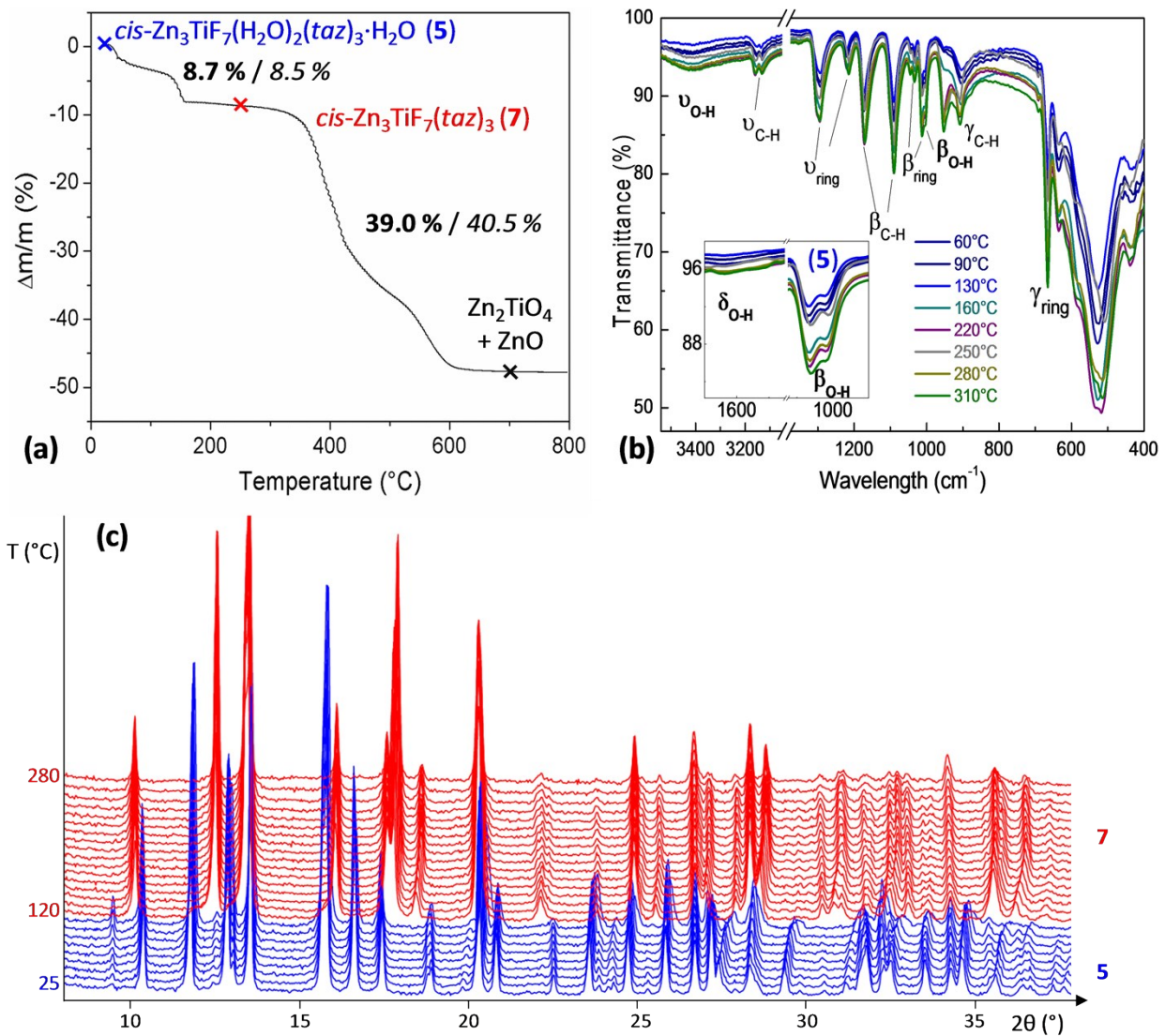


Fig. S3. (a) TGA under humid air atmosphere, (b) thermal evolution of IR spectra and (c) thermal evolution of the powder X-Ray diffractograms of 5. Color code: blue = $cis\text{-Zn}_3\text{TiF}_7(\text{H}_2\text{O})_2(\text{taz})_3\cdot\text{H}_2\text{O}$ (5), red = $cis\text{-Zn}_3\text{TiF}_7(\text{taz})_3$ (7).

3. DFT calculations

Light atoms, and H atoms in particular, are difficult to locate accurately using XRD data. Optimization of atomic positions (APO) by DFT is a possible method to obtain more reliable H positions. For the ordered phases **1**, **3** and **7**, the highest atomic displacements between experimental (ES) and APO structures are effectively observed for protons (see Tables S1, S2 and S4). The structures of phases **4** and **5** present partial atomic occupancies, preventing DFT calculations. Then ordered structures have been constructed. For phase **4**, an ordered structure, named **4o**, was generated in the non-centrosymmetric Pn₂₁a space group. As a result, the sites affected by the space group change present the highest atomic displacements (see Table S3). Phase **5** presents partial occupancies for two water molecules located in cavities; the sites are labelled OW2 (0.69) and OW3 (0.713). The atomic position optimization was performed on an ordered structure, labelled **5p**, with empty W2 and full W3 water sites. Unsurprisingly, the atoms of these water molecules are the most affected by the atomic position optimization (see Table S5).

Table S1. Experimental (x , y , z) and PBE-DFT geometry-optimized (x' , y' , z') fractional atomic coordinates, and corresponding atomic displacements (d , Å) for phase **1**.

Atom	Site	x	y	z	x'	y'	z'	d
Zn1	2a	0.55313	0	0.50946	0.55615	0	0.51536	0.048
Zn2	4b	0.066	0.33878	0.1719	0.07002	0.33967	0.17469	0.042
Ti1	2a	0	0	0	-0.00162	0	-0.00562	0.045
F1	2a	0.1112	0.50	0.3078	0.12556	0.50	0.31355	0.146
F2	4b	-0.0049	0.17288	-0.0042	-0.00575	0.17369	-0.01082	0.056
F3	2a	-0.0717	0	-0.2371	-0.07834	0	-0.24654	0.084
F4	2a	0.167	0	0.0035	0.16613	0	-0.01116	0.126
F5	2a	0.0659	0	0.23	0.07065	0	0.22912	0.050
F6	2a	-0.1725	0	-0.0249	-0.17353	0	-0.02357	0.012
N1	4b	0.0264	0.43672	-0.0366	0.02684	0.43685	-0.03509	0.012
N2	2a	0.5092	0	0.7168	0.5096	0	0.71827	0.012
N3	4b	0.42698	0.20061	0.2451	0.42948	0.19814	0.2445	0.037
N4	4b	0.4193	0.1415	0.3782	0.42152	0.14036	0.3773	0.026
N5	4b	0.24349	0.26242	0.2564	0.24556	0.26077	0.25426	0.029
C1	4b	0.0157	0.4027	-0.1853	0.01614	0.40198	-0.18444	0.011
C2	4b	0.3085	0.1806	0.3799	0.31032	0.1798	0.37989	0.022
C3	4b	0.3208	0.2711	0.1753	0.32273	0.26906	0.17261	0.033
OW1	4b	0.70439	0.13657	0.6061	0.70507	0.14006	0.60342	0.044
OW2	2a	0.9689	0	0.4632	0.98471	0	0.46595	0.168
OW3	4b	0.1493	0.1537	-0.2764	0.14692	0.15628	-0.27983	0.041
H1	4b	0.0129	0.3211	-0.2186	0.0165	0.30631	-0.21997	0.165
H2	4b	0.2784	0.1546	0.4574	0.27593	0.15079	0.4713	0.121
H3	4b	0.3018	0.3205	0.0819	0.30283	0.32779	0.06515	0.164
HW1A	4b	0.784	0.107	0.679	0.79312	0.10488	0.67234	0.096
HW1B	4b	0.727	0.188	0.543	0.69151	0.21277	0.66337	0.999
HW2A	2a	0.97	0	0.362	1.00345	0	0.36644	0.359
HW2B	2a	0.8814	0	0.435	0.88897	0	0.42734	0.082
HW3A	4b	0.212	0.099	-0.215	0.1664	0.11152	-0.17569	0.496
HW3B	4b	0.083	0.105	-0.344	0.08189	0.10527	-0.37093	0.233

Table S2. Experimental (x , y , z) and PBE-DFT geometry-optimized (x' , y' , z') fractional atomic coordinates, and corresponding atomic displacements (d , Å) for phase **3**.

Atom	Site	x	y	z	x'	y'	z'	d
Zn1	2a	0.2567	0	0.4394	0.25991	0	0.43959	0.036
Zn2	4b	-0.0449	0.3326	-0.1998	-0.0413	0.33329	-0.1997	0.041
Ti	2a	0	0	0	-0.0009	0	-0.0081	0.058
F1	2a	0.4201	0	-0.3587	0.42947	0	-0.3543	0.103
F2	4b	-0.0079	-0.1716	-0.0099	-0.0055	-0.1796	0.0007	0.115
F3	2a	0.0894	0	0.2455	0.08411	0	0.25329	0.073
F4	2a	0.1476	0	-0.0815	0.14924	0	-0.0724	0.066
F5	2a	-0.0806	0	-0.2518	-0.0798	0	-0.2544	0.020
F6	2a	-0.1463	0	0.0739	-0.1516	0	0.06825	0.064
N1	4b	-0.0499	0.4355	0.0302	-0.0521	0.43577	0.02512	0.040
N2	2a	0.3606	0	0.226	0.36119	0	0.25156	0.187
N3	4b	-0.2126	0.2716	-0.3017	-0.2131	0.27713	-0.3073	0.072
N4	4b	-0.2909	0.3444	0.5581	-0.2903	0.34507	0.55827	0.009
N5	4b	0.0921	0.2771	-0.3036	0.09716	0.27829	-0.3044	0.057
C1	4b	-0.0977	0.3987	0.1716	-0.1043	0.39993	0.1625	0.090
C2	4b	0.6035	0.3058	0.5623	0.59661	0.30997	0.56342	0.088
C3	4b	0.2093	0.2995	-0.236	0.21694	0.29619	-0.2277	0.100
H1	4b	-0.1039	0.3103	0.2114	-0.1177	0.30217	0.19461	0.196
H2	4b	0.527	0.3369	0.4763	0.51583	0.35034	0.47458	0.189
H3	4b	0.234	0.3559	-0.1243	0.2527	0.36153	-0.1154	0.214

Table S3. Experimental (x , y , z) and PBE-DFT geometry-optimized (x' , y' , z') fractional atomic coordinates, and corresponding atomic displacements (d , Å) for phase **4o**.

Atom	Site	x	y	z	x'	y'	z'	d
Zn1	4a	0.1220	0.25	0.3075	0.1151	0.24927	0.31101	0.124
Zn2	4a	0.2996	0.4208	0.3772	0.2961	0.41584	0.38728	0.138
Zn2B	4a	-0.2996	-0.4208	-0.3772	-0.29519	-0.42085	-0.38646	0.128
Ti1	4a	0.4425	0.75	0.2972	0.44183	0.73902	0.30210	0.126
F1	4a	0.2355	0.25	0.3991	0.2306	0.24727	0.41295	0.179
F2	4a	0.3712	0.6145	0.3351	0.36954	0.60399	0.33878	0.119
F2'	4a	-0.3712	-0.6145	-0.3351	-0.37311	-0.62415	-0.34546	0.156
F3	4a	0.3966	0.75	0.1443	0.39251	0.75135	0.14833	0.084
F4	4a	0.5145	0.8719	0.247	0.5178	0.86547	0.25881	0.158
F4'	4a	-0.5145	-0.8719	-0.247	-0.5124	-0.88329	-0.23623	0.172
F5	4a	0.4775	0.75	0.4486	0.48037	0.72743	0.45429	0.246
N1	4a	-0.1044	0.3177	0.1635	-0.108	0.31139	0.15385	0.140
N1B	4a	0.1044	-0.3177	-0.1635	0.10903	-0.32165	-0.15961	0.099
N2	4a	0.0126	0.25	0.2227	0.0075	0.24543	0.22208	0.099
N3	4a	0.2385	0.4676	0.2303	0.23631	0.46095	0.2382	0.118
N3B	4a	-0.2385	-0.4676	-0.2303	-0.23582	-0.46937	-0.23947	0.114
N4	4a	0.171	0.399	0.202	0.17276	0.38728	0.20558	0.131
N4B	4a	-0.171	-0.399	-0.202	-0.16657	-0.40745	-0.21261	0.166
N5	4a	0.2953	0.4844	0.5444	0.29479	0.48186	0.55313	0.102
N5B	4a	-0.2953	-0.4844	-0.5444	-0.29347	-0.49072	-0.55102	0.103
C1	4a	-0.0341	0.3515	0.1987	-0.03733	0.34822	0.19133	0.105
C1B	4a	0.0341	-0.3515	-0.1987	0.03913	-0.35811	-0.20081	0.112
C1E	4a	0.6755	0.75	0.0852	0.67379	0.74481	0.0887	0.072
C2	4a	0.1533	0.4305	0.0923	0.15614	0.41839	0.09381	0.135
C2B	4a	-0.1533	-0.4305	-0.0923	-0.14976	-0.43892	-0.10086	0.143
C2E	4a	0.6144	0.7692	-0.0098	0.61168	0.77857	-0.00274	0.133
C3	4a	0.2561	0.5356	0.134	0.25515	0.53385	0.144	0.115
C3B	4a	-0.2561	-0.5356	-0.134	-0.25763	-0.53544	-0.14255	0.099
O1E	4a	0.5623	0.8764	0.0343	0.56069	0.88247	0.03768	0.078
OW1	4a	0.0856	0.3923	0.4327	0.07775	0.4223	0.41729	0.378
OW1'	4a	-0.0856	-0.3923	-0.4327	-0.07323	-0.35932	-0.45075	0.448
H1	4a	-0.0181	0.4375	0.2064	-0.01938	0.44907	0.19805	0.153
H1AB	4a	-0.061	-0.47	-0.43	-0.07759	-0.45566	-0.45632	0.434
H1B	4a	0.0181	-0.4375	-0.2064	0.02247	-0.45884	-0.21486	0.251
H1BB	4a	-0.065	-0.357	-0.499	-0.0859	-0.32128	-0.5301	0.619
H1E	4a	0.55551	0.88103	0.10659	0.54583	0.86591	0.12239	0.288
H1E1	4a	0.7219	0.7926	0.04588	0.71195	0.82776	0.10871	0.810
H1E2	4a	0.68717	0.67722	0.12085	0.71094	0.66595	0.05482	0.852
H1E3	4a	0.6588	0.82016	0.1447	0.64657	0.71176	0.17218	1.176
H1WA	4a	0.061	0.47	0.43	0.06256	0.49496	0.36536	0.769
H1WB	4a	0.065	0.357	0.499	0.02938	0.40331	0.46417	0.864
H2	4a	0.11	0.3977	0.0516	0.10877	0.37526	0.04274	0.252
H2B	4a	-0.11	-0.3977	-0.0516	-0.09874	-0.40321	-0.05295	0.200
H2E1	4a	0.58276	0.66376	0.00808	0.57506	0.69351	-0.02387	0.489
H2E2	4a	0.63214	0.74639	-0.08563	0.63817	0.81346	-0.0862	0.698
H3	4a	0.2991	0.591	0.1286	0.30259	0.60436	0.1437	0.226
H3B	4a	-0.2991	-0.591	-0.1286	-0.31007	-0.59545	-0.13693	0.214

Table S4. Experimental (x , y , z) and PBE-DFT geometry-optimized (x' , y' , z') fractional atomic coordinates, and corresponding atomic displacements (d , Å) for phase **7**.

Atom	Site	x	y	z	x'	y'	z'	d
Zn1	4c	0.1417	0.25	0.319	0.13806	0.25	0.3333	0.157
Zn2	8d	0.3236	0.4214	0.3264	0.32216	0.42559	0.3315	0.071
Ti1	4c	0.420	0.75	0.2038	0.44421	0.75	0.20034	0.426
F1	4c	0.256	0.25	0.352	0.25729	0.25	0.38145	0.295
F2	8d	0.3724	0.5831	0.256	0.37631	0.61204	0.26694	0.319
F3	4c	0.374	0.75	0.0283	0.37473	0.75	0.0358	0.076
F4	8d	0.4965	0.8469	0.1121	0.50355	0.87683	0.12185	0.341
F5	4c	0.4771	0.75	0.363	0.49297	0.75	0.36195	0.279
N1	8d	-0.0825	0.1835	0.246	-0.09186	0.18193	0.23825	0.182
N2	4c	0.032	0.25	0.288	0.02271	0.25	0.3003	0.204
N3	8d	0.241	0.474	0.2167	0.23401	0.4731	0.21471	0.125
N4	8d	0.171	0.419	0.2182	0.16646	0.40498	0.20868	0.188
N5	8d	0.3091	0.503	0.5211	0.32085	0.47908	0.5215	0.318
C1	8d	-0.0159	0.3501	0.279	-0.02259	0.35574	0.27663	0.133
C2	8d	0.1423	0.444	0.1057	0.13511	0.4355	0.0912	0.210
C3	8d	0.2509	0.514	0.0983	0.23972	0.54255	0.10207	0.351
H1	8d	-0.0011	0.4301	0.3104	-0.00613	0.45849	0.2916	0.354
H2	8d	0.0931	0.4412	0.0916	0.08173	0.39508	0.05452	0.627
H3	8d	0.2807	0.5965	0.086	0.28723	0.6077	0.07936	0.174

Table S5. Experimental (x , y , z) and PBE-DFT geometry-optimized (x' , y' , z') fractional atomic coordinates, and corresponding atomic displacements (d , Å) for phase **5p**.

Atom	Site	x	y	z	x'	y'	z'	d
Zn1	4c	0.1215	0.25	0.2967	0.12778	0.25	0.26672	0.353
Zn2	8d	0.2949	0.4212	0.3641	0.29935	0.42283	0.33603	0.324
Ti1	4c	0.4416	0.75	0.2698	0.45287	0.75	0.25575	0.249
F1	4c	0.2221	0.25	0.3937	0.23544	0.25	0.36277	0.415
F2	8d	0.3747	0.6041	0.3250	0.38165	0.61238	0.29135	0.404
F3	4c	0.3988	0.75	0.1156	0.41502	0.75	0.09978	0.329
F4	8d	0.5014	0.8858	0.2120	0.53094	0.87629	0.21111	0.515
F5	4c	0.4892	0.75	0.4130	0.48487	0.75	0.41305	0.074
N1	8d	-0.1105	0.3183	0.1712	-0.10310	0.31722	0.16779	0.133
N2	4c	0.0160	0.25	0.2220	0.01971	0.25	0.17930	0.483
N3	8d	0.2358	0.4880	0.2047	0.24435	0.46817	0.18656	0.322
N4	8d	0.1684	0.4117	0.2025	0.17848	0.39736	0.16030	0.524
N5	8d	0.2931	0.5037	0.5278	0.28668	0.49288	0.49867	0.362
C1	8d	-0.0366	0.3605	0.1850	-0.02883	0.35416	0.17414	0.191
C2	8d	0.1524	0.4270	0.0885	0.16126	0.42270	0.04761	0.485
C3	8d	0.2608	0.5437	0.1049	0.26385	0.53428	0.08811	0.218
OW1	8d	0.0767	0.4080	0.4165	0.08767	0.40088	0.38295	0.427
OW3	8d	0.5732	0.8704	0.0350	0.55934	0.88609	-0.04055	0.894
H1	8d	-0.0247	0.4480	0.2287	-0.01092	0.45619	0.17748	0.626
H1WA	8d	0.0610	0.4700	0.4300	0.07953	0.48000	0.33372	1.130
H1WB	8d	0.0650	0.3570	0.4990	0.03310	0.38337	0.41343	1.136
H2	8d	0.1204	0.3635	0.0515	0.11199	0.38008	0.00043	0.614
H3	8d	0.2889	0.6346	0.0931	0.31289	0.60172	0.08163	0.545
H3WA	8d	0.5632	0.8604	0.0450	0.57733	0.97694	-0.03421	1.502
H3WB	8d	0.5832	0.8804	0.0250	0.55480	0.86037	0.04352	0.566

Table S6. Selected interatomic distances (\AA) from ES and APO structures of phase 1.

ES				APO			
F1	Zn2	2x	2.0585	F1	Zn2	2x	2.0647
	Zn1	1x	2.1501		Zn1	1x	2.2376
F2	Ti1	1x	1.8772	F2	Ti1	1x	1.8859
	Zn2	1x	2.2867		Zn2	1x	2.3352
					H1	1x	2.4427
F3	HW1A	2x	1.8628	F3	HW1A	2x	1.7281
	Ti1	1x	1.8944		Ti1	1x	1.9229
F4	Ti1	1x	1.8576	F4	HW3A	2x	1.8953
	HW3A	2x	2.4498		Ti1	1x	1.9011
F5	Ti1	1x	1.8405	F5	HW2A	1x	1.6857
	HW2A	1x	1.9006		Ti1	1x	1.8748
F6	Ti1	1x	1.8473	F6	Ti1	1x	1.8622
	H3	2x	2.2383		H3	2x	2.0886

Table S7. Selected interatomic distances (\AA) from ES and APO structures of phase 3.

ES				APO			
F1	Zn1	1x	2.0943	F3	Zn2	2x	2.0951
	Zn2	2x	2.1208		Zn1	1x	2.1602
F2	Ti	1x	1.8285	F1	Ti1	1x	1.9133
	Zn2	1x	2.1938		Zn2	1x	2.1813
F3	Ti	1x	1.8687	F4	Ti1	1x	1.9551
	Zn1	1x	2.0966		Zn1	1x	2.1432
					H1	1x	2.4689
F4	Ti	1x	1.8765	F5	Ti1	1x	1.8427
	Ti	1x	1.8797	F6	Ti1	1x	1.8393
F6	Ti	1x	1.8347	F7	Ti1	1x	1.8900
	H3	2x	2.3312		H3	2x	2.1271

Table S8. Selected interatomic distances (\AA) from ES and APO structures of phase **4o**.

ES				APO			
F1	Zn2	1x	2.0834	F1	Zn2B	1x	2.0714
	Zn2B	1x	2.0834		Zn2	1x	2.0823
	Zn1	1x	2.1879		Zn1	1x	2.2740
F2	Ti1	1x	1.8969	F2	Ti1	1x	1.9011
	Zn2	1x	2.3837		Zn2	1x	2.3681
	H2B	1x	2.4518		H2B	1x	2.4625
					H3	1x	2.4664
F3	Ti1	1x	1.8841	F3	H1BB	1x	1.5657
	H1WB	1x	2.0723		Ti1	1x	1.9218
	H1BB	1x	2.0723		H3B	1x	2.1146
	H3	1x	2.3372		H3	1x	2.1525
	H3B	1x	2.3372				
F4	H1E	1x	1.7248	F4	H1E	1x	1.6024
	Ti1	1x	1.8419		Ti1	1x	1.8977
	H1B	1x	2.1045		H1B	1x	1.9561
F5	Ti1	1x	1.7991	F5	Ti1	1x	1.8321
	H2	1x	2.4213		H2B	1x	2.2011
	H2B	1x	2.4213		H2	1x	2.3665
F6	Ti1	1x	1.8969	F6	Ti1	1x	1.8942
	Zn2B	1x	2.3837		H2	1x	2.2335
	H2	1x	2.4518				
F7	Ti1	1x	1.8419	F7	Ti1	1x	1.8902
	H1	1x	2.1045		H1WA	1x	1.8964
					H1	1x	1.9526

Table S9. Selected interatomic distances (\AA) from ES and APO structures of phase **7**.

ES				APO			
F1	Zn1	1x	2.0334	F1	Zn1	1x	2.1476
	Zn2	2x	2.1130		Zn2	2x	2.1644
F2	Ti1	1x	1.9509	F2	Ti1	1x	1.9496
	Zn2	1x	1.9722		Zn2	1x	2.2041
	H3	1x	2.3425		H3	1x	2.4394
F3	Ti1	1x	1.9284	F3	Zn1	1x	2.0336
	Zn1	1x	2.1066		Ti1	1x	2.0454
	H3	2x	2.3266		H3	2x	2.1471
F4	Ti1	1x	1.8965	F4	Ti1	1x	1.8265
	F4	1x	1.9556		H1	1x	1.8805
	H1	1x	2.3798				
F5	Ti1	1x	1.8784	F5	Ti1	1x	1.8257

Table S10. Selected interatomic distances (\AA) from ES and APO structures of phase **5p**.

ES				APO			
F1	Zn1	1x	2.0359	F1	Zn2	2x	2.0934
	Zn2	2x	2.1680		Zn1	1x	2.1335
F2	Ti1	1x	1.9749	F2	Ti1	1x	1.8993
	Zn2	1x	2.3504		H2	1x	2.3476
	H1	1x	2.4189		Zn2	1x	2.4411
F3	H1wB	2x	1.8109	F3	Ti1	1x	1.8645
	Ti1	1x	1.8773		H3	2x	2.3182
	H3	2x	2.2310				
	F4	2x	2.4822				
F4	Ti1	1x	1.8381	F4	H1wA	1x	1.7564
	H1	1x	1.8720		Ti1	1x	1.9205
	H3wA	1x	2.1656		H3wB	1x	1.9294
	Ow3	1x	2.3390		H1	1x	2.2321
	H1wA	1x	2.3937				
	F3	1x	2.4822				
	Ti1	1x	1.8001				
				F5	Ti1	1x	1.8464
					H2	2x	2.3368

Table S11. Phase, H site and multiplicity, ^1H σ_{iso} (ppm) issued from DFT-GIPAW calculations, H environment, weighted average ^1H σ_{iso} ($\langle \sigma_{\text{iso}} \rangle$, ppm) and its relative intensity (%) for APO structures.

Phase	H site	Mult.	σ_{iso}	H env.	$\langle \sigma_{\text{iso}} \rangle$	Intensity
1	H W2B	2	29.8	water in cavities	25.5	62.5
	H W3A	4	27.4	water in cavities		
	H W2A	2	25.6	water in cavities		
	H W3B	4	25.5	water in cavities		
	H W1A	4	25.0	Zn bonded water		
	H W1B	4	22.1	Zn bonded water		
	H2	4	22.1	Taz		
	H3	4	21.3	Taz	21.4	37.5
3	H1	4	20.8	Taz	21.4	100
	H3	4	22.0	Taz		
	H1	4	21.8	Taz		
4o	H2	4	20.5	Taz	29.0	37.5
	H3E3	4	31.0	Ethanol		
	H3E2	4	30.9	Ethanol		
	H3E1	4	30.6	Ethanol		
	H2E2	4	30.0	Ethanol		
	H2E1	4	27.5	Ethanol		
	H1E	4	24.4	Ethanol		
	H W1A	4	27.4	water in cavities		
	H W1B	4	24.1	water in cavities	24.2	25.0
	H W1AB	4	23.2	water in cavities		
	H W1BB	4	22.2	water in cavities		
	H2	4	20.9	Taz	20.6	37.5
	H2B	4	20.9	Taz		
	H3	4	20.8	Taz		
	H3B	4	20.4	Taz		
	H1	4	20.3	Taz		
	H1B	4	20.2	Taz	26.2	57.1
7	H2	8	22.1	Taz		
	H3	8	20.3	Taz	20.7	100
	H1	8	19.8	Taz		
5p	H6	8	28.5	water in cavities	20.9	42.9
	H7	8	28.2	water in cavities		
	H1	8	26.3	Zn bonded water		
	H2	8	22.0	Zn bonded water		
	H3	8	21.2	Taz		
	H5	8	20.8	Taz		
	H4	8	20.7	Taz		

Table S12. Phase, F site and multiplicity, $^{19}F \sigma_{iso}$ and σ_{csa} (ppm) issued from DFT-GIPAW calculations, F environment, weighted average $^{19}F \sigma_{iso}$ ($\langle \sigma_{iso} \rangle$, ppm) and its relative intensity (%) for APO structures.

Phase	F site	Mult.	σ_{iso}	σ_{csa}	F env.	$\langle \sigma_{iso} \rangle$	Intensity
1	F1	2	343.5	6.8	Zn ₃	343.5	14.3
	F3	2	64.3	198.4	Ti		
	F4	2	32.0	267.5	Ti		
	F2	4	21.1	272.5	TiZn	15.7	85.7
	F5	2	2.8	296.7	Ti		
	F6	2	-46.7	312.1	Ti		
3	F1	2	322.8	13.4	Zn ₃	322.8	14.3
	F3	2	135.7	184.3	TiZn		
	F2	4	82.9	217.4	TiZn		
	F6	2	-1.9	291.9	Ti	24.3	85.7
	F4	2	-60.5	378.9	Ti		
	F5	2	-93.2	368.0	Ti		
4o	F1	4	357.5	-16.0	Zn ₃	357.5	14.3
	F3	4	68.0	204.0	Ti		
	F2	4	41.0	252.4	TiZn		
	F4	4	24.5	235.2	Ti	11.6	85.7
	F6	4	15.0	272.3	TiZn		
	F7	4	6.4	283.2	Ti		
	F5	4	-85.6	387.8	Ti		
7	F1	4	331.9	26.0	Zn ₃	331.9	14.3
	F3	4	215.2	101.9	TiZn		
	F2	8	120.6	199.2	TiZn	35.0	85.7
	F5	4	-110.6	414.3	Ti		
	F4	8	-120.6	398.2	Ti		
5p	F1	4	353.9	14.1	Zn ₃	353.9	14.3
	F4	8	59.5	232.2	Ti		
	F2	8	31.6	259.0	TiZn	13.3	85.7
	F3	4	-37.2	321.4	Ti		
	F5	4	-65.3	374.8	Ti		

4. ^1H MAS NMR

All spectra were reconstructed with the DMFIT¹software.

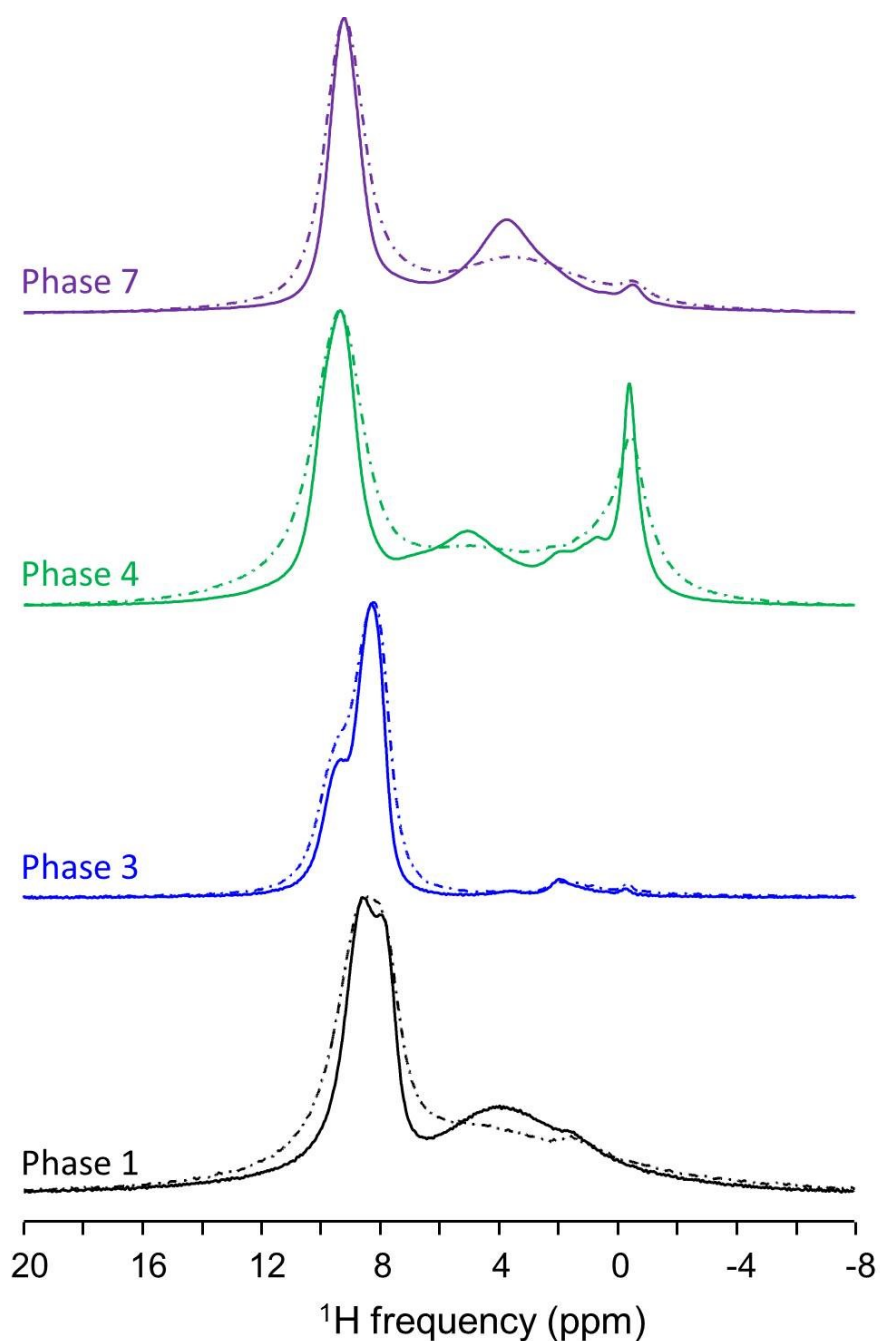


Fig. S4. Experimental ^1H MAS NMR (7 T) spectra of phases **1** (black), **3** (blue), **4** (green) and **7** (violet) recorded at 64 kHz (solid lines) and 44 kHz (dashed lines) spinning frequencies.

¹ D. Massiot, F. Fayon, M. Capron, I. King, S. Le Calvé, B. Alonso, J.-O. Durand, B. Bujoli, Z. Gan and G. Hoatson, *Magn. Reson. Chem.*, 2002, **40**, 70–76.

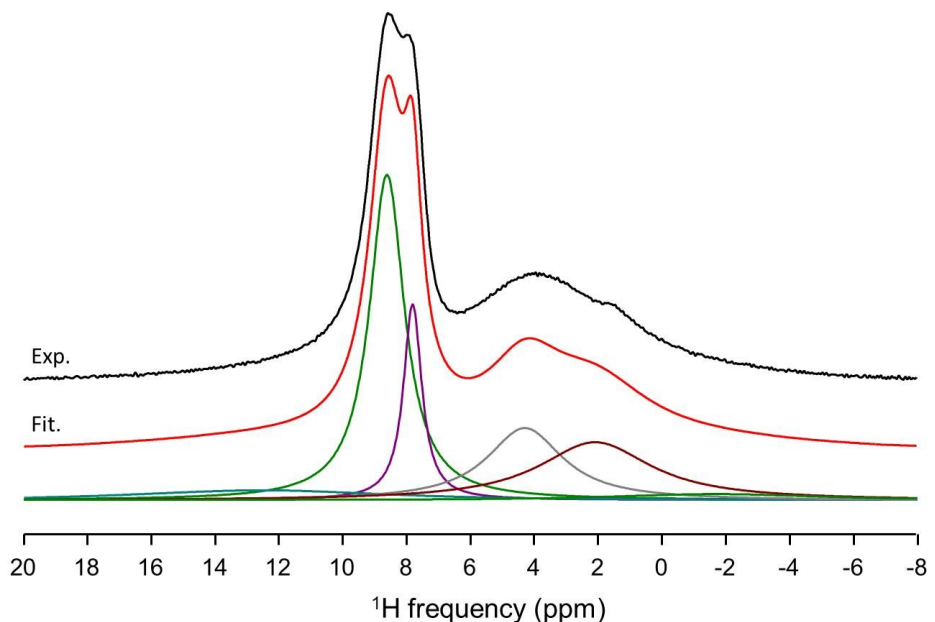


Fig. S5. Experimental (black) and fitted (red) ^1H MAS (64 kHz) NMR (7 T) spectra of phase **1**. The individual contributions to the reconstructed spectrum are shown below (see Table S13).

Table S13. ^1H isotropic chemical shift (δ_{iso} , ppm), line width (LW, ppm), relative intensity (I, %), weighted average δ_{iso} values ($\langle \delta_{\text{iso}} \rangle$, ppm) and its corresponding relative intensity (I, %) determined from reconstruction of the ^1H NMR spectrum of phase **1**.

Line	δ_{iso} (± 0.1)	LW (± 0.2)	I (± 1)	$\langle \delta_{\text{iso}} \rangle$ (± 0.1)	I (± 1)
1	12.5	9.2	6.6		
2	8.6	1.3	38.2	8.9	56.8
3	7.8	0.7	12.0		
4	4.3	2.9	18.3		
5	2.1	4.3	21.9	2.7	43.3
6	-1.7	7.7	3.1		

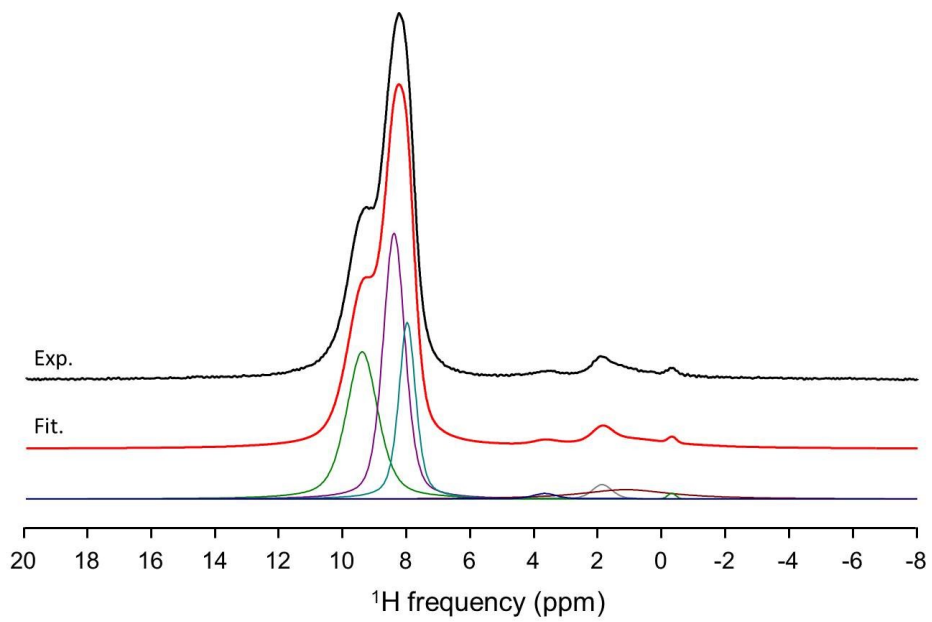


Fig. S6. Experimental (black) and fitted (red) ^1H MAS (64 kHz) NMR (7 T) spectra of phase **3**. The individual contributions to the reconstructed spectrum are shown below (see Table S14).

Table S14. ^1H isotropic chemical shift (δ_{iso} , ppm), line width (LW, ppm), relative intensity (I, %), weighted average δ_{iso} values ($\langle \delta_{\text{iso}} \rangle$, ppm) and its corresponding relative intensity (I, %) determined from reconstruction of the ^1H NMR spectrum of phase **3**.

Line	δ_{iso} (± 0.1)	LW (± 0.2)	I (± 1)	$\langle \delta_{\text{iso}} \rangle$ (± 0.1)	I (± 1)
1	9.4	1.2	31.6		
2	8.4	0.8	38.1	8.7	90.1
3	8.0	0.6	20.3		
4	3.7	0.9	0.7		
5	1.9	0.7	1.8	1.4	9.9
6	1.2	3.5	7.2		
7	-0.3	0.3	0.3		

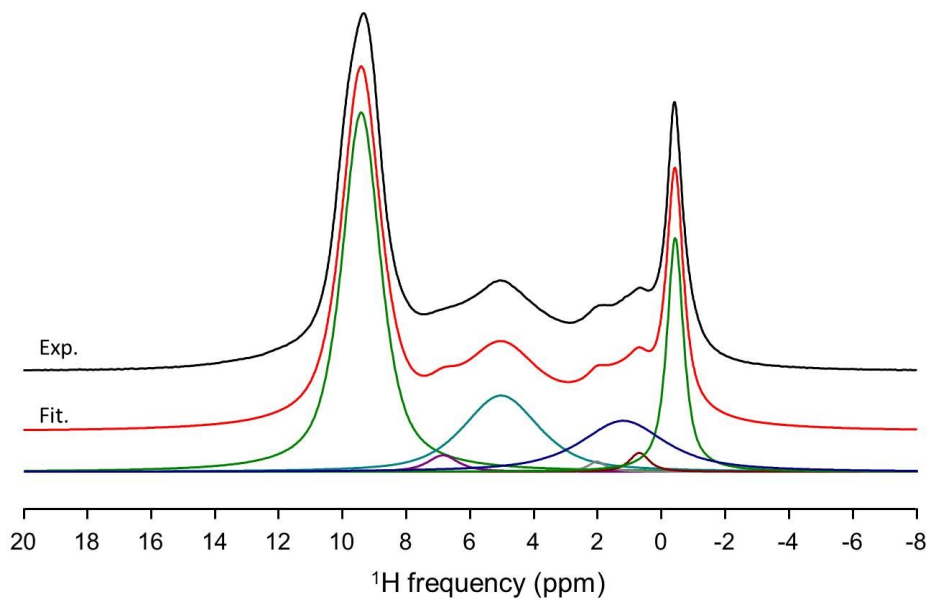


Fig. S7. Experimental (black) and fitted (red) ^1H MAS (64 kHz) NMR (7 T) spectra of phase **4**. The individual contributions to the reconstructed spectrum are shown below (see Table S15).

Table S15. ^1H isotropic chemical shift (δ_{iso} , ppm), line width (LW, ppm), relative intensity (I, %), weighted average δ_{iso} values ($\langle \delta_{\text{iso}} \rangle$, ppm) and its corresponding relative intensity (I, %) determined from reconstruction of the ^1H NMR spectrum of phase **4**.

Line	δ_{iso} (± 0.1)	LW (± 0.2)	I (± 1)	$\langle \delta_{\text{iso}} \rangle$ (± 0.1)	I (± 1)
1	9.4	1.4	47.4	9.4	47.4
2	6.9	1.1	1.7	5.2	21.3
3	5.0	2.8	19.6		
4	2.0	0.7	0.7		
5	1.2	3.2	15.7		
6	0.7	0.7	1.3	0.5	31.2
7	-0.4	0.6	13.5		

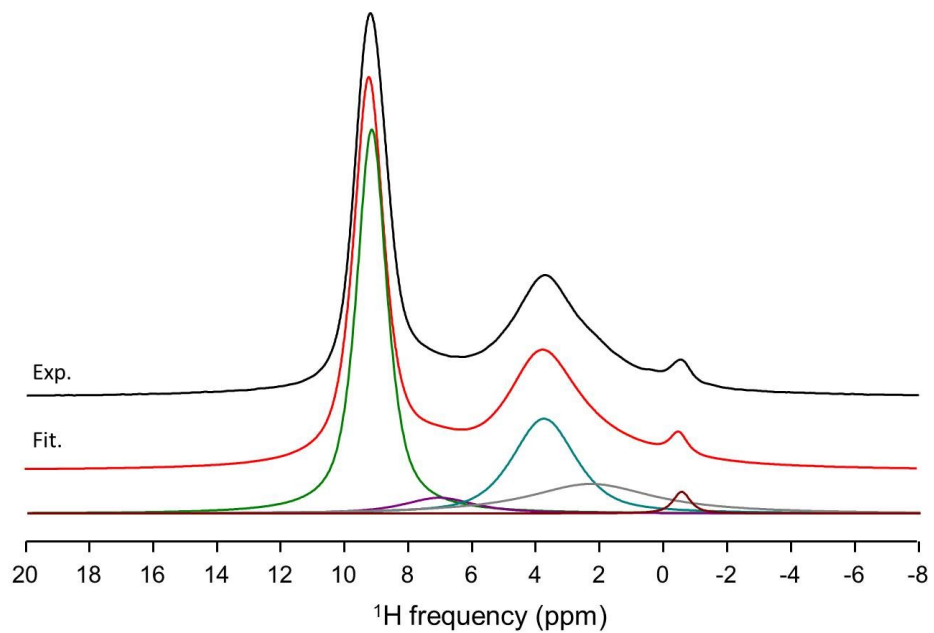


Fig. S8. Experimental (black) and fitted (red) ¹H MAS (64 kHz) NMR (7 T) spectra of phase 7. The individual contributions to the reconstructed spectrum are shown below (see Table S16).

Table S16. ¹H isotropic chemical shift (δ_{iso} , ppm), line width (LW, ppm), relative intensity (I, %), weighted average δ_{iso} values ($\langle \delta_{\text{iso}} \rangle$, ppm) and its corresponding relative intensity (I, %) determined from reconstruction of the ¹H NMR spectrum of phase 7.

Line	δ_{iso} (± 0.1)	LW (± 0.2)	I (± 1)	$\langle \delta_{\text{iso}} \rangle$ (± 0.1)	I (± 1)
1	9.2	1.1	48.5	9.1	51.5
2	7.6	1.6	3.0		
3	3.7	3.0	45.7	3.4	48.5
4	-0.5	0.9	2.8		

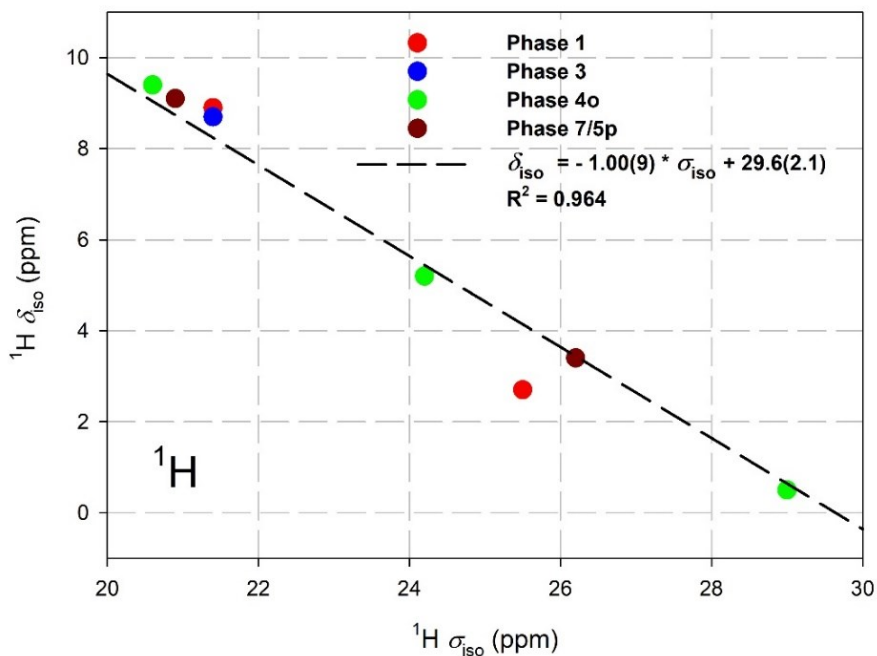
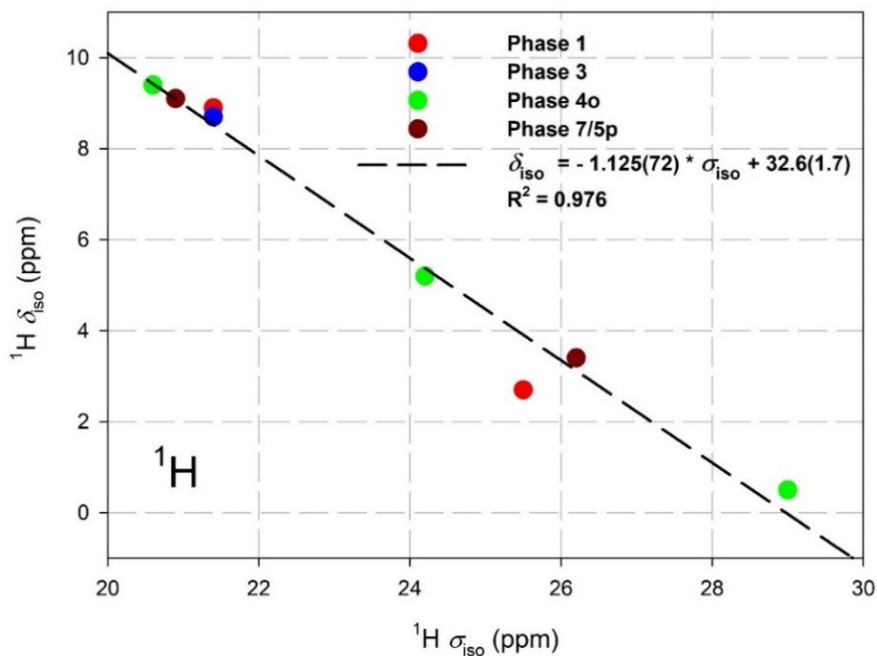


Fig. S9. Top and bottom: ${}^1\text{H} \sigma_{\text{iso,cal}}$ weighted average values versus ${}^1\text{H} \delta_{\text{iso,exp}}$ weighted average values. The dashed black line represents the linear regression calculated on these values and corresponds to the equation reported on the graph. **Top:** fitted slope. The slope of the linear correlation (-1.125) deviates a little from the theoretical -1 value. **Bottom:** slope kept to the theoretical value of minus one. In both cases, the ${}^1\text{H} \sigma_{\text{ref}}$ value is quite similar to one previously determined (31 ppm).²

² C. Gervais, M. Profeta, V. Lafond, C. Bonhomme, T. Azaïs, H. Mutin, C. J. Pickard, F. Mauri, F. Babonneau, *Magn. Reson. Chem.* 2004, **42**, 445–452.

5. ^{19}F MAS NMR

All spectra were reconstructed with the DMFIT¹ software.

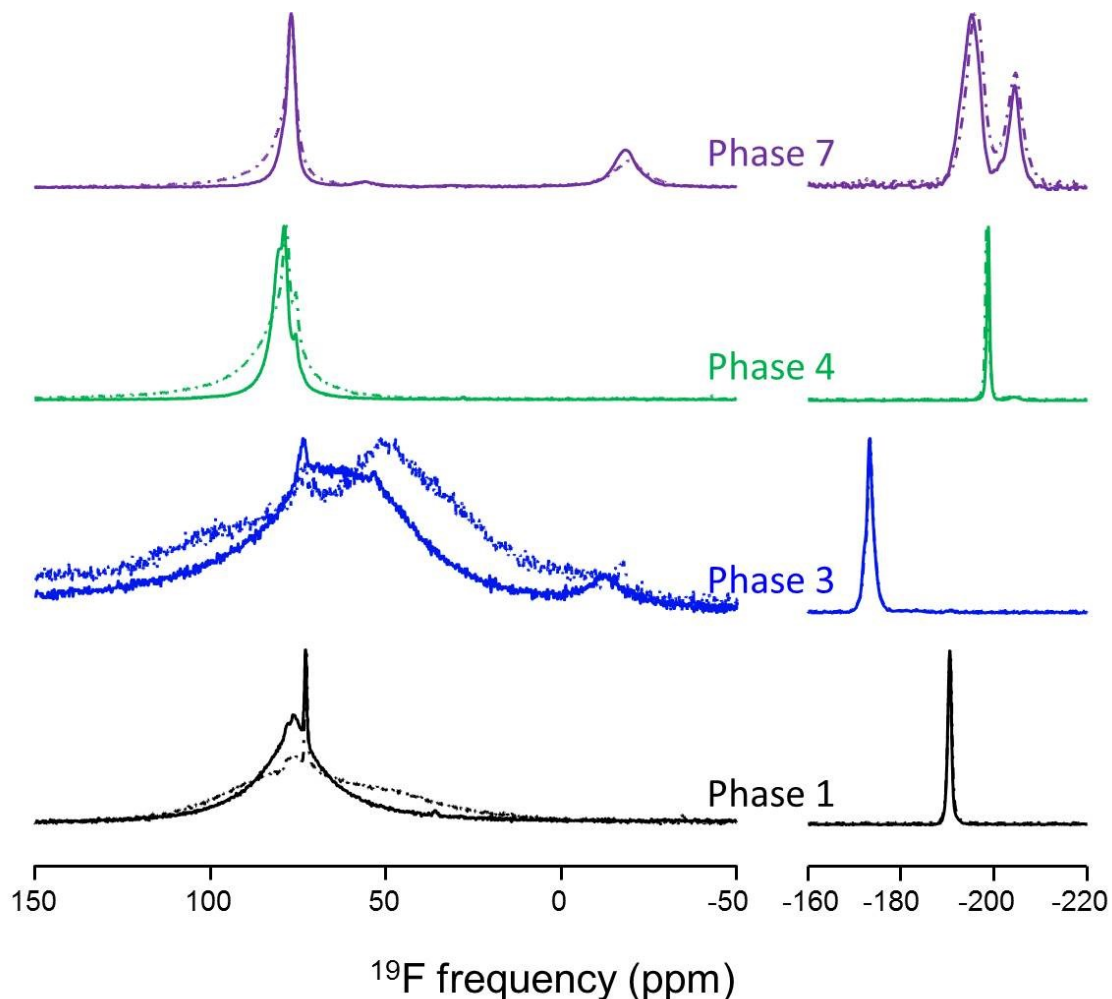


Fig. S10. Experimental ^{19}F MAS NMR (7 T) spectra of phases **1** (black), **3** (blue) **4** (green) and **7** (violet) recorded at 64 kHz (solid lines) and 44 kHz (dashed lines) spinning frequencies.

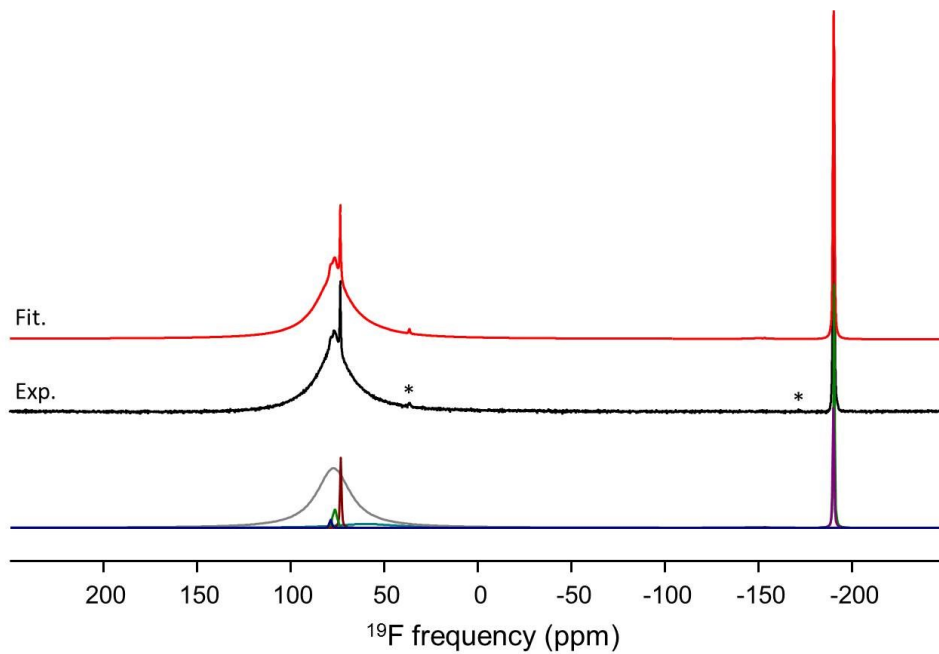


Fig. S11. Experimental (black) and fitted (red) ^{19}H MAS (64 kHz) NMR (7 T) spectra of phase **1**. The individual contributions to the reconstructed spectrum are shown below (see Table S17). The asterisks indicate spinning sidebands.

Table S17. ^{19}F isotropic chemical shift (δ_{iso} , ppm), chemical shift anisotropy (δ_{csa} , ppm), asymmetry parameter (η), line width (LW, ppm), relative intensity (I, %), weighted average ^{19}F δ_{iso} values ($\langle \delta_{\text{iso}} \rangle$, ppm) and its corresponding relative intensity (I, %) determined from reconstruction of the ^{19}F NMR spectrum of phase **1**.

Line	δ_{iso} (± 0.1)	δ_{csa} (± 10)	η (± 0.1)	LW (± 0.2)	I (± 1)	$\langle \delta_{\text{iso}} \rangle$ (± 0.1)	I (± 1)
1	-190.5	-100	0	0.7	8.7	-190.4	
2	-190.2	-100	0	0.8	5.4	14.1	
3	59.7	-100	0	39.9	8.1		
4	73.1	-100	0	0.7	3.1		
5	76.3	-100	0	2.8	2.2	75.2	
6	77.0	-100	0	21.8	71.9	85.9	
7	78.5	-100	0	1.6	0.6		

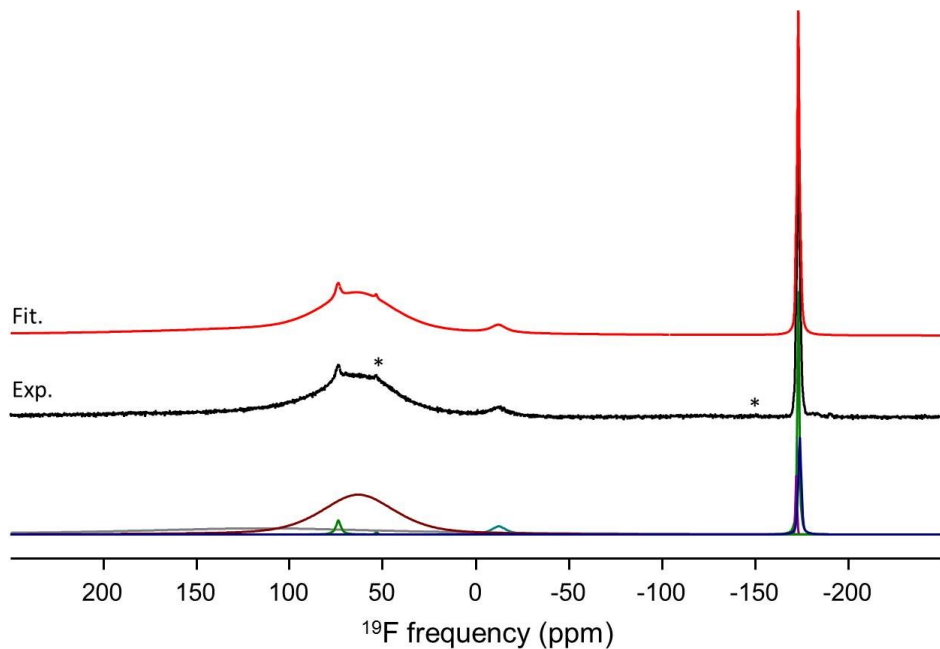


Fig. S12. Experimental (black) and fitted (red) ^{19}H MAS (64 kHz) NMR (7 T) spectra of phase **3**. The individual contributions to the reconstructed spectrum are shown below (see Table S18). The asterisks indicate spinning sidebands.

Table S18. ^{19}F isotropic chemical shift (δ_{iso} , ppm), chemical shift anisotropy (δ_{csa} , ppm), asymmetry parameter (η), line width (LW, ppm), relative intensity (I , %), weighted average ^{19}F δ_{iso} values ($\langle \delta_{\text{iso}} \rangle$, ppm) and its corresponding relative intensity (I , %) determined from reconstruction of the ^{19}F NMR spectrum of phase **3**.

Line	δ_{iso} (± 0.1)	δ_{csa} (± 10)	η (± 0.1)	LW (± 0.2)	I (± 1)	$\langle \delta_{\text{iso}} \rangle$ (± 0.1)	I (± 1)
1	-173.9	50	1	1.9	5.2		
2	-173.2	-100	0	1.1	9.1	-173.3	15.6
3	-172.0	50	1	1.0	1.4		
4	-12.2	50	1	9.8	2.6		
5	63.2	50	1	46.7	50.9	79.1	84.4
6	73.9	50	1	3.1	1.5		
7	114.8	50	1	179.4	29.4		

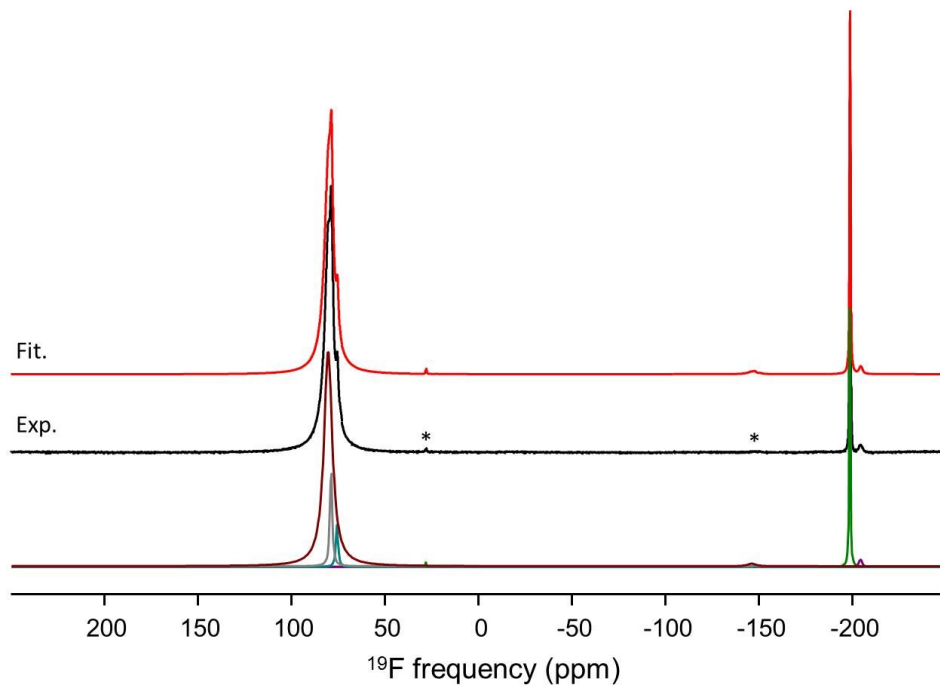


Fig. S13. Experimental (black) and fitted (red) ^{19}H MAS (64 kHz) NMR (7 T) spectra of phase 4. The individual contributions to the reconstructed spectrum are shown below (see Table S19). The asterisks indicate spinning sidebands.

Table S19. ^{19}F isotropic chemical shift (δ_{iso} , ppm), chemical shift anisotropy (δ_{csa} , ppm), asymmetry parameter (η), line width (LW, ppm), relative intensity (I , %), weighted average ^{19}F δ_{iso} values ($\langle \delta_{\text{iso}} \rangle$, ppm) and its corresponding relative intensity (I , %) determined from reconstruction of the ^{19}F NMR spectrum of phase 4.

Line	δ_{iso} (± 0.1)	δ_{csa} (± 10)	η (± 0.1)	LW (± 0.2)	I (± 1)	$\langle \delta_{\text{iso}} \rangle$ (± 0.1)	I (± 1)
1	-204.4	-100	0	2.2	0.9	-204.4	0.9
2	-198.7	-100	0	0.7	13.5	-198.7	13.5
3	75.5	-100	0	1.5	3.8		
4	78.7	-100	0	1.5	8.9	79.9	85.7
5	80.3	-100	0	5.3	72.9		

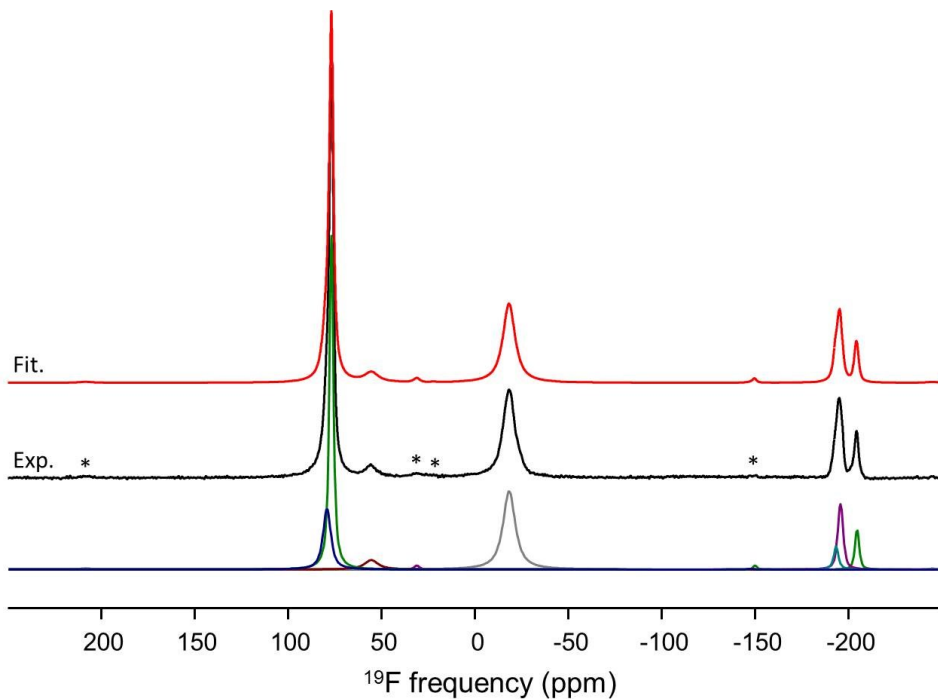


Fig. S14. Experimental (black) and fitted (red) ^{19}H MAS (64 kHz) NMR (7 T) spectra of phase **7**. The individual contributions to the reconstructed spectrum are shown below (see Table S20). The asterisks indicate spinning sidebands.

Table S20. ^{19}F isotropic chemical shift (δ_{iso} , ppm), chemical shift anisotropy (δ_{csa} , ppm), asymmetry parameter (η), line width (LW, ppm), relative intensity (I, %), weighted average ^{19}F δ_{iso} values ($\langle \delta_{\text{iso}} \rangle$, ppm) and its corresponding relative intensity (I, %) determined from reconstruction of the ^{19}F NMR spectrum of phase **7**.

Line	δ_{iso} (± 0.1)	δ_{csa} (± 10)	η (± 0.1)	LW (± 0.2)	I (± 1)	$\langle \delta_{\text{iso}} \rangle$ (± 0.1)	I (± 1)
1	-204.3	-100	0	2.7	4.5	-204.3	4.5
2	-195.4	-200	0	3.4	10.1	-194.9	13.2
3	-193.1	-100	0	3.0	3.1		
4	-18.2	-100	0	7.8	27.7		
5	55.5	-100	0	8.8	4.0	44.2	82.3
6	76.8	-100	0	2.5	37.4		
7	79.2	-100	0	5.0	13.3		

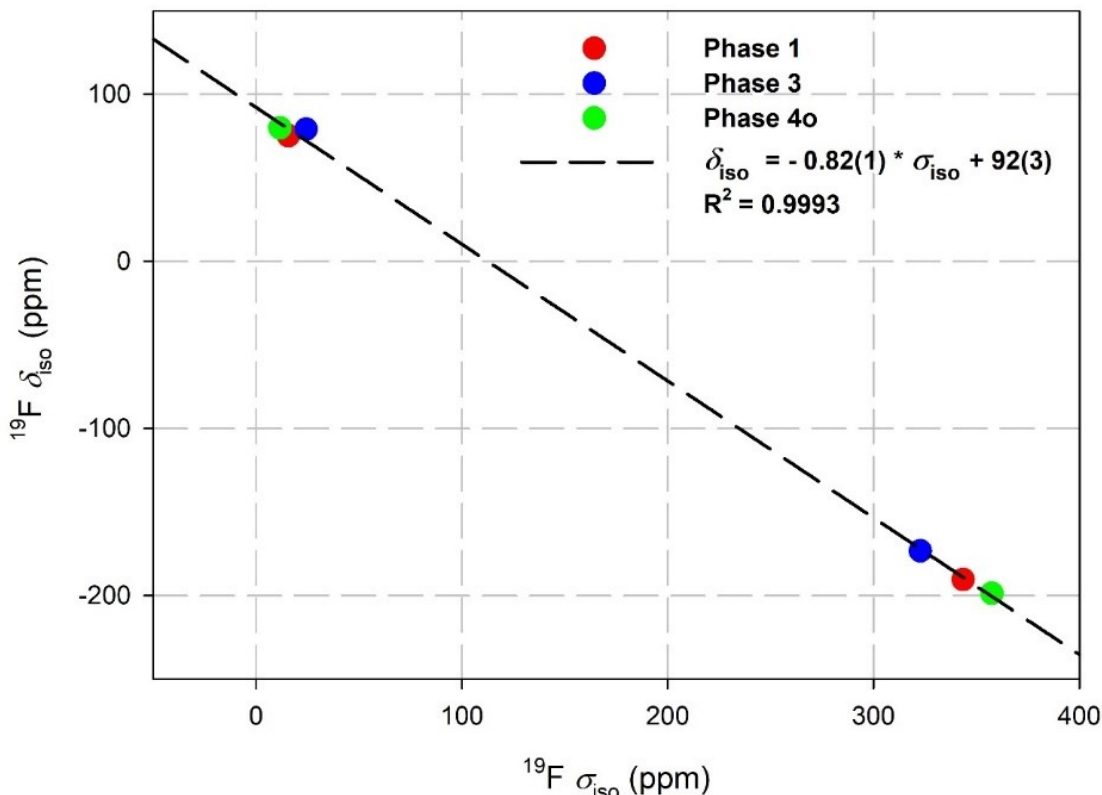


Fig. S15. $^{19}\text{F} \sigma_{\text{iso},\text{cal}}$ weighted average values versus $^{19}\text{F} \delta_{\text{iso},\text{exp}}$ weighted average values. The dashed black line represents the linear regression calculated on these values and corresponds to the equation reported on the graph.

The equation of the linear correlation is quite close to the one established on basic fluorides ($\delta_{\text{iso},\text{cal}} = -0.795 \sigma_{\text{iso},\text{cal}} + 89$),³ far from the one established on TiF_4 ($\delta_{\text{iso},\text{cal}} = -1.128 \sigma_{\text{iso},\text{cal}} + 63$)⁴ whereas the linear correlation ($\delta_{\text{iso},\text{cal}} = -0.97 \sigma_{\text{iso},\text{cal}} + 67$) determined on hybrid oxyfluorotitanates is in-between.⁵ In the studied phases, F atoms are either FZn_3 or FTiZn or are terminal F ones whereas in $[\text{H}_2\text{taz}]_2 \cdot (\text{Ti}_5\text{O}_5\text{F}_{12})$ and $[\text{H}_2\text{gua}]_2 \cdot (\text{Ti}_5\text{O}_5\text{F}_{12})$ as in TiF_4 , only F atoms bridging two Ti atoms or terminal F atoms are encountered.^{4,5}

3 A. Sadoc, M. Biswal, M. Body, C. Legein, F. Boucher, D. Massiot, F. Fayon, *Solid State Nucl. Magn. Reson.*, 2014, **59–60**, 1–7.

4 M. Murakami, Y. Noda, K. Takegoshi, *Solid State Nucl. Magn. Reson.*, 2019, **101**, 82–88.

5 M. Albino, M. Body, C. Legein, A. Hemon-Ribaud, M. Leblanc, V. Maisonneuve, J. Lhoste, *Cryst Growth Des.*, 2018, **18**, 6873–6884.

Table S21. Experimental (*x*, *y*, *z*) fractional atomic coordinates for phase **2**.

Atom	Site	<i>x</i>	<i>y</i>	<i>z</i>
Zn1	2a	0.5272(8)	0	0.5228(9)
Zn2	4b	0.0556(6)	0.3407(5)	0.1801(8)
Ti1	2a	0	0	0
F1	2a	0.076(3)	1/2	0.312(2)
F2	4b	-0.022(2)	0.1746(8)	0.007(2)
F3	2a	-0.006(4)	0	-0.222(2)
F4	2a	0.1740(13)	0	0.037(4)
F5	2a	0.036(4)	0	0.2266(17)
F6	2a	-0.1660(16)	0	-0.004(4)
N1	4b	0.033(4)	0.4374(6)	-0.0190(18)
N2	2a	0.483(2)	0	0.7323(16)
N3	4b	0.4134(13)	0.2087(11)	0.2421(17)
N4	4b	0.4033(12)	0.1521(13)	0.3771(16)
N5	4b	0.2451(11)	0.2927(15)	0.2686(19)
C1	4b	0.027(3)	0.4032(10)	-0.1678(15)
C2	4b	0.2980(14)	0.2016(15)	0.384(2)
C3	4b	0.3307(10)	0.3032(9)	0.1987(15)
OW1	4b	0.676(2)	0.143(2)	0.602(3)

Table S22. Experimental (*x*, *y*, *z*) fractional atomic coordinates for phase **6**.

Atom	Site	<i>x</i>	<i>y</i>	<i>z</i>
Zn1	4a	0.1257(2)	1/4	0.2761(3)
Zn2	4a	0.29567(15)	0.42985(20)	0.33396(19)
Ti1	4a	0.4418(3)	3/4	0.2463(5)
F1	4a	0.2412(6)	1/4	0.3515(11)
F2	4a	0.3718(5)	0.6066(7)	0.2862(6)
F3	4a	0.4016(6)	3/4	0.0983(10)
F4	4a	0.5153(5)	0.8782(6)	0.1858(7)
F5	4a	0.4865(7)	3/4	0.3913(9)
N1	4a	-0.10499(12)	0.319426(7)	0.1825(10)
N2	4a	0.01857(15)	1/4	0.1923(17)
N3	4a	0.2331(4)	0.4662(10)	0.1817(3)
N4	4a	0.1645(3)	0.3987(10)	0.1652(2)
N5	4a	0.2906(4)	0.4975(11)	0.4957(2)
C1	4a	-0.03094(12)	0.3541(4)	0.2029(15)
C2	4a	0.1554(5)	0.4252(13)	0.0484(3)
C3	4a	0.2578(5)	0.5343(12)	0.0852(4)
OW1	4a	0.0943(5)	0.4100(10)	0.4044(8)
HW1		0.0830	0.4976	0.4051
HW2		0.0555	0.3679	0.4587
H1	4a	-0.0156	0.4432	0.19877
H2	4a	0.1070	0.3957	0.0070
H3B	4a	0.3002	0.5862	0.0795